Subwavelength superdirective gyrotropic cylindrical nanoantenna

V. A. Es'kin*

Department of Radiophysics, University of Nizhny Novgorod, 23 Gagarin Avenue, Nizhny Novgorod 603950, Russia

(Received 11 February 2021; accepted 14 July 2021; published 5 August 2021)

Electromagnetic radiation of a nanoantenna formed by a magnetic-current filament of infinite length and an electrically thin multilayer gyrotropic cylindrical scatterer in the surrounding free space is studied. It is shown the possibility to achieve simultaneously high directivity of radiation and the desired direction of the main lobe of the antenna radiation pattern by choosing the parameters of the layers of the gyrotropic cylinder. It is demonstrated that the radiation field of such an antenna in the far zone has a nonzero angular momentum with respect to the cylinder axis. A comparison is made between the radiation characteristics of such an antenna and the radiation characteristics of an antenna of similar geometry with isotropic filling of a multilayer cylindrical scatterer.

DOI: 10.1103/PhysRevA.104.023505

I. INTRODUCTION

Owing to recent advances in metamaterials and nanotechnology, it becomes possible to create unique nanoscale electromagnetic emitting systems with previously unattainable capabilities [1]. Such nanoantennas can excite electromagnetic fields with the desired characteristics, which are defined by the application area [2–4]. One of these characteristics is high directivity, which plays an important role in many applications, in particular, single-photon nanoantennas [5,6], optical communication in nanocircuits [7,8], near-field subwavelength imaging [9], and photonic artificial neural networks [10]. However, a high degree of directivity of an antenna is usually associated with their large effective size [11]. In recent works [6,12–18], possible configurations of radiation sources have been shown, which have a large directivity and electrically small sizes simultaneously.

In Refs. [6,15–18] it is presented that nanoantenna formed by parallel filamentary current and a multilayer dielectric cylinder of electrically small transverse size can have a directional pattern with a high level of the main lobe and low levels of the side lobes. These results were achieved through careful optimization of the parameters of the cylinder layers. The maximum of the radiation pattern of these antenna systems can be achieved in the plane in which the filamentary current and the cylinder axis lie (i.e., forward or backward directions). An attempt to choose the parameters of an antenna system with the main lobe of the directional pattern directed at a certain angle to the mentioned plane did not lead to the desired result because, in addition to the sought main lobe, a mirrored lobe of the directional pattern appeared relatively to the plane of symmetry of the antenna. This disadvantage is explained by the fact that the cylinder is formed by layers filled with isotropic media. Such a cylinder scatters the electromagnetic field of the filamentary current into azimuthal harmonics (modes) with the same efficiency if the azimuthal indices coincide in absolute value. This drawback can be avoided by replacing isotropic media with gyrotropic ones. As it was shown earlier [19,20], gyrotropic cylindrical scatterers have several features, the most interesting of which are the selective excitation of individual azimuthal harmonics and the ability to control the characteristics of scattering (and medium parameters) by varying the external magnetic field. In this work, the radiation of electromagnetic waves from a magnetic current of infinity length in the presence of a multilayer gyrotropic cylindrical scatterer is considered. The emphasis is placed on the possibility of forming the high directivity in the desired direction by choosing the appropriate permittivities of the layers of the cylinder.

II. FORMULATION OF THE PROBLEM AND BASIC EQUATIONS

Consider a cylinder, which consists of a circularly cylindrical core of radius ρ_1 covered with $N-1$ concentric layers with the outer radius ρ_j $(j=2,\ldots,N)$ (see Fig. 1) and located in free space. The cylinder is infinitely long and aligned with the z axis of a cylindrical coordinate system (ρ,ϕ,z). Every jth region is filled with a gyrotropic medium, which is characterized by a permittivity tensor,

$$\hat{\varepsilon}_j=\epsilon_0\begin{pmatrix}\varepsilon_j & -ig_j & 0\\ ig_j & \varepsilon_j & 0\\ 0 & 0 & \eta_j\end{pmatrix}, \tag{1}$$

where ϵ_0 is the electric constant. The permittivity tensor (1) describes, for example, an indium antimonide (InSb) [21–23] and a gyrotropic metamaterial [24,25] in the optical and infrared ranges and a magnetoplasma in the radio-frequency range [26,27]. The gyrotropic media are magnetized with an external static magnetic field that is aligned with the cylinder.

We study the scattering of electromagnetic waves excited by a filamentary source aligned with the z axis. The magnetic current density of the source, with the $\exp(i\omega t)$ time dependence dropped, in a cylindrical coordinate system (ρ_s,ϕ_s,z)

*vasiliy.eskin@gmail.com

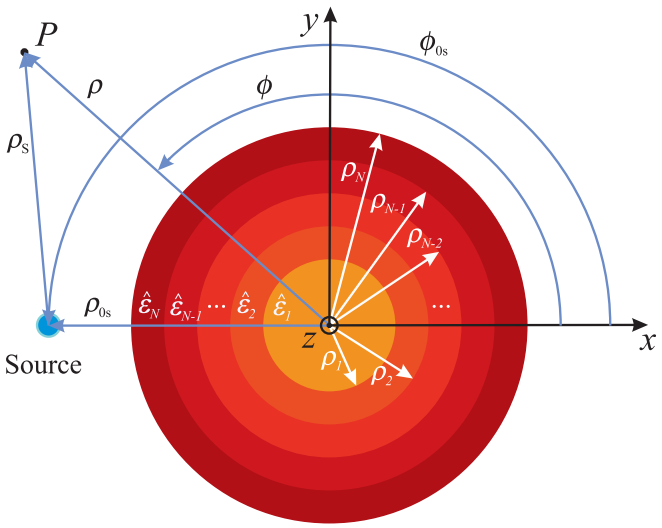

FIG. 1. Geometry of the problem. P is the observation point; ρ and ϕ stand for the radial and azimuthal coordinates of this point, respectively, in the coordinate system (ρ, ϕ, z) related to the multilayer cylindrical scatterer; ρ_s and ϕ_s are coordinates of this point in the coordinate system (ρ_s, ϕ_s, z) related to the source; and the zero subscript is used to designate the source position in the coordinate system of the cylinder.

related to the source is written as [19]

$$\mathbf{J} = \mathbf{z}_0 I_0 \delta(\rho_s)/(2\pi\rho_s), \tag{2}$$

where δ is the Dirac function, and I_0 is the total magnetic current of the filamentary source. It is assumed that the wavelength $\lambda = 2\pi/k_0$ in the surrounding medium is much longer than the cylinder's outer radius ρ_N (here, $k_0 = \omega/c$ is the wave number in free space, ω is the angular frequency, and c is the speed of light in free space).

The longitudinal magnetic-field component excited by the magnetic-current filament (2) can be written as

$$H_z^{(f)} = -Z_0^{-1} I_0 k_0 H_0^{(2)}(k_0\rho_s)/4. \tag{3}$$

Hereafter, Z_0 is the wave impedance of free space, $H_m^{(2)}$ is the Hankel function of the second kind of order m, and the superscript (f) denotes that the corresponding quantity refers to the field excited by the filamentary source.

The field in the inner regions of the cylinder, as well as the field scattered from and incident on it, can conveniently be represented in a cylindrical coordinate system in terms of azimuthal harmonics with the indices $m = 0, \pm1, \pm2, \ldots$ as follows:

$$\begin{bmatrix}\mathbf{E}\\ \mathbf{H}\end{bmatrix} = \sum_{m=-\infty}^{\infty} \begin{bmatrix}\mathbf{E}_m\\ \mathbf{H}_m\end{bmatrix} \exp(-im\phi). \tag{4}$$

In turn, the vector quantities $\mathbf{E}_m$ and $\mathbf{H}_m$ can be expressed via the longitudinal magnetic-field component $H_{z;j,m}$ in the jth region of the cylinder, which satisfies the following equation in the gyrotropic media [27]:

$$\frac{d^2 H_{z;j,m}}{d\rho^2} + \frac{1}{\rho}\frac{dH_{z;j,m}}{d\rho} + \left(k_0^2 q_j^2 - \frac{m^2}{\rho^2}\right) H_{z;j,m} = 0. \tag{5}$$

Here, $q_j = [(\varepsilon_j^2 - g_j^2)/\varepsilon_j]^{1/2}$ is the normalized (to k_0) transverse (to cylinder axis) wave number of the extraordinary wave in the gyrotropic medium of the jth region, and the electric-field components $E_{\rho;j,m}$ and $E_{\phi;j,m}$ are expressed via the longitudinal magnetic-field component $H_{z;j,m}$ [27]:

$$E_{\rho;j,m} = -\frac{Z_0}{k_0(\varepsilon_j^2 - g_j^2)}\left(\frac{m\varepsilon_j}{\rho} H_{z;j,m} + g_j \frac{dH_{z;j,m}}{d\rho}\right), \tag{6}$$

$$E_{\phi;j,m} = \frac{iZ_0}{k_0(\varepsilon_j^2 - g_j^2)}\left(\frac{m g_j}{\rho} H_{z;j,m} + \varepsilon_j \frac{dH_{z;j,m}}{d\rho}\right). \tag{7}$$

To obtain the field outside the cylinder, one should put $\varepsilon_j = 1$, $g_j = 0$, and $\eta_j = 1$ in Eqs. (5)–(7).

The components of the field inside the core of the cylinder are represented in the following forms:

$$E_{\rho;1,m} = -\frac{B_m}{\varepsilon_1 q_1}\left[\frac{m\varepsilon_1}{k_0\rho} J_m(k_0 q_1 \rho) + q_1 g_1 J_m'(k_0 q_1 \rho)\right],$$

$$E_{\phi;1,m} = i\frac{B_m}{\varepsilon_1 q_1}\left[\frac{m g_1}{k_0\rho} J_m(k_0 q_1 \rho) + q_1 \varepsilon_1 J_m'(k_0 q_1 \rho)\right],$$

$$H_{z;1,m} = Z_0^{-1} B_m q_1 J_m(k_0 q_1 \rho), \tag{8}$$

where J_m is the Bessel function of the first kind of order m, and B_m is the amplitude coefficient corresponding to the azimuthal index m. Hereafter, the prime indicates the derivative with respect to the argument.

The components of the field inside the jth region of the cylinder ($j > 1$) are represented in the following forms:

$$E_{\rho;j,m} = -\sum_{k=1}^{2} \frac{C_{j,m}^{(k)}}{\varepsilon_j q_j}\left[\frac{m\varepsilon_j}{k_0\rho} H_m^{(k)}(k_0 q_j \rho) + q_j g_j H_m^{(k)\prime}(k_0 q_j \rho)\right],$$

$$E_{\phi;j,m} = i\sum_{k=1}^{2} \frac{C_{j,m}^{(k)}}{\varepsilon_j q_j}\left[\frac{m g_j}{k_0\rho} H_m^{(k)}(k_0 q_j \rho) + q_j \varepsilon_j H_m^{(k)\prime}(k_0 q_j \rho)\right],$$

$$H_{z;j,m} = Z_0^{-1}\sum_{k=1}^{2} C_{j,m}^{(k)} q_j H_m^{(k)}(k_0 q_j \rho), \tag{9}$$

where $H_m^{(1)}$ is the Hankel function of the first kind of order m, and $C_{j,m}^{(1)}$ and $C_{j,m}^{(2)}$ are the amplitude coefficients corresponding to the azimuthal index m.

The total field outside the cylinder is a superposition of the scattered and incident-wave fields. The components of the field scattered from the cylinder, which are denoted by the superscript (s), are written as

$$E_{\rho;m}^{(s)} = -D_m \frac{m}{k_0\rho} H_m^{(2)}(k_0\rho),$$

$$E_{\phi;m}^{(s)} = iD_m H_m^{(2)\prime}(k_0\rho),$$

$$H_{z;m}^{(s)} = Z_0^{-1} D_m H_m^{(2)}(k_0\rho), \tag{10}$$

where D_m is the scattering coefficient corresponding to the azimuthal index m.

The azimuthal harmonics of the field radiated from the magnetic-current filament can be rewritten in the coordinate system related to the cylinder with the help of Graf's addition

theorem for cylindrical functions [28]:

$$H_0^{(2)}(k_0\rho_s)=\sum_{m=-\infty}^{\infty} J_m(k_0\rho)H_m^{(2)}(k_0\rho_{0s})e^{-im(\phi-\phi_{0s})}, \quad (11)$$

under the condition $\rho \leqslant \rho_{0s}$. Here, ρ_{0s} and ϕ_{0s} are the source coordinates in the coordinate system of the cylinder. To obtain representation of the Hankel function $H_0^{(2)}(k_0\rho_s)$ in the region $\rho > \rho_{0s}$, it is necessary to replace the arguments of the Bessel function by $k_0\rho_{0s}$ and of the Hankel function by $k_0\rho$ in the right side of Eq. (11). As a result, the components of the source-excited field in this system are represented in the following forms:

$$\begin{aligned} E_{\rho;m}^{(f)} &= -A_m \frac{m}{k_0\rho} J_m(k_0\rho)H_m^{(2)}(k_0\rho_{0s}), \\ E_{\phi;m}^{(f)} &= iA_m J_m'(k_0\rho)H_m^{(2)}(k_0\rho_{0s}), \\ H_{z;m}^{(f)} &= Z_0^{-1}A_m J_m(k_0\rho)H_m^{(2)}(k_0\rho_{0s}), \end{aligned} \quad (12)$$

for the case of $\rho \leqslant \rho_{0s}$. Here the coefficient A_m is written as

$$A_m = -I_0 \frac{k_0}{4}\exp(im\phi_{0s}). \quad (13)$$

The components of the source-excited field in the region $\rho > \rho_{0s}$ can be obtained via replacing the arguments of the Bessel function and its derivative with $k_0\rho_{0s}$ and the arguments of the Hankel function and its derivative with $k_0\rho$ in the right sides of Eqs. (12).

The coefficients B_m, $C_{j,m}^{(1)}$, $C_{j,m}^{(2)}$, and D_m are then determined from the conditions of continuity of the tangential field components at the surface of each layer.

Further, we focus mostly on directivity, which is the ratio of time-averaged radiation power in a given direction to the radiated power averaged over all directions. Directivity of the considered radiating system is given by (see detailed derivation in Appendix A)

$$D(\phi)=\frac{\left|\sum_{m=-\infty}^{\infty} i^m[A_m J_m(k_0\rho_{0s})+D_m]\exp(-im\phi)\right|^2}{\sum_{m=-\infty}^{\infty}|A_m J_m(k_0\rho_{0s})+D_m|^2}. \quad (14)$$

III. NUMERICAL RESULTS

Consider a five-layer cylindrical scatterer, whose exterior radius has a value of $\rho_5 = 0.1\lambda$ and the inner radii are fixed on values $\rho_1 = 0.02\lambda$, $\rho_2 = 0.04\lambda$, $\rho_3 = 0.06\lambda$, and $\rho_4 = 0.08\lambda$. The magnetic-current filament is located at the distance $\rho_{0s} = 1.05\rho_5$ from the axis of a cylindrical scatterer and at an angle $\phi_{0s} = 180^\circ$. We paid the main attention to choosing such a combination of the elements of the permittivity tensors (1) of the cylinder layers at which the maximum directivity is achieved in the direction $\phi_{\max}$. The optimization procedure and the results obtained are given in Appendix B. The numerical calculations were carried out at azimuthal indexes limited to $m = 0, \pm1, \ldots, \pm5$ instead of the infinite number of the terms summed over the azimuthal index in Eq. (4). Note that this antenna configuration is superdirective at a directivity greater than 1.257 [15]. Because the antenna configuration and presented results are defined in terms of λ, they can scale to different frequency ranges. For example, in the optical frequency range for a source operating at a wavelength $\lambda = 600$ nm, a cylindrical nanoantenna has an exterior radius of 60 nm. State-of-the-art technologies [29] allow fabricating such thin multilayer structures based on an indium antimonide.

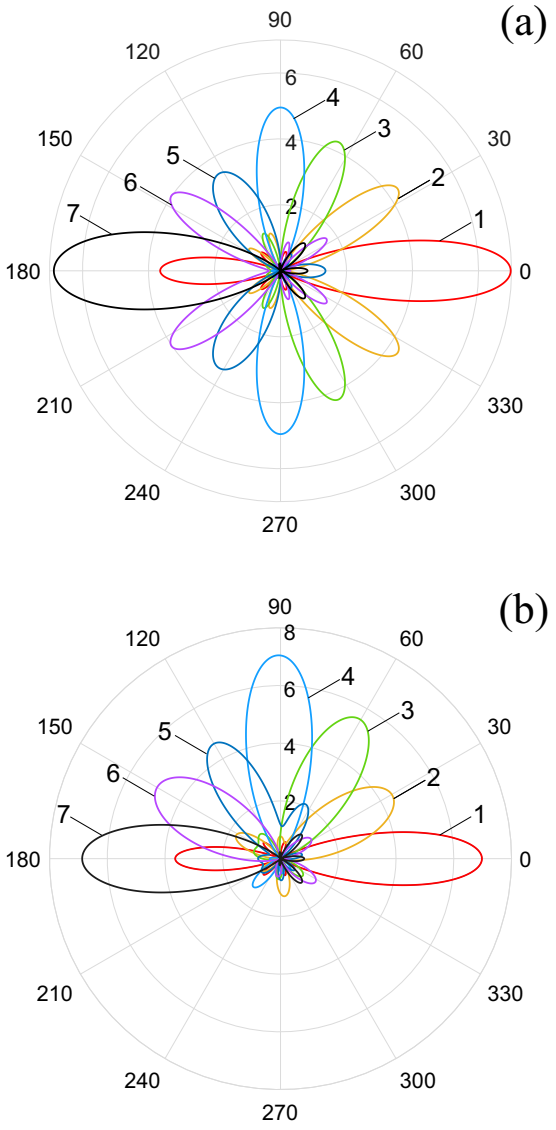

FIG. 2. (a) Directivities obtained for the case of the isotropic media of layers of the cylinder. The numbers of curves correspond to the numbers of examples of media of layers, for which the elements of the permittivity tensors are given in Table I. (b) Directivities were obtained for the case of the gyrotropic media of layers of the cylinder. The numbers of curves correspond to the numbers of examples of media of layers, for which the elements of the permittivity tensors are given in Table II.

At first, we studied the directivity of an antenna of the taken geometry in the case of filling the layers of a cylinder with isotropic media. Isotropic medium is described by the simplest permittivity tensor (1) which has identical diagonal elements ($\eta_j = \varepsilon_j$) and off-diagonal elements are absent ($g_j = 0$). Figure 2(a) shows several directivities obtained as a result of the optimization procedure for the following desired directions of the maximum radiation: $\phi_{\max}^{\text{ex.1}} = 0^\circ$, $\phi_{\max}^{\text{ex.2}} =$

30°, $\phi_{\max}^{\text{ex.3}} = 60^\circ$, $\phi_{\max}^{\text{ex.4}} = 90^\circ$, $\phi_{\max}^{\text{ex.5}} = 120^\circ$, $\phi_{\max}^{\text{ex.6}} = 150^\circ$, and $\phi_{\max}^{\text{ex.7}} = 180^\circ$ (here the superscript "ex.n" denotes that this value refers to the nth curve (example) shown in the given figure). The found parameters of the media at which the distributions were plotted in Fig. 2(a) are given in the Table I. As you can see from Fig. 2(a), the desired directions of the directivity maxima for the examples noted above, examples 2, 3, 5, and 6, differ from the received directions, which are $\phi_{\max}^{\text{ex.2}} = 34.6^\circ$, $\phi_{\max}^{\text{ex.3}} = 65.9^\circ$, $\phi_{\max}^{\text{ex.5}} = 122.8^\circ$, and $\phi_{\max}^{\text{ex.6}} = 145.1^\circ$. Another feature of the scattering field of the magnetic-current source from an isotropic cylinder is the appearance of the addition maximum. For example, in addition to the main lobe in the direction $\phi_{\max}^{\text{ex.2}} = 34.6^\circ$, the lobe appears in the direction $\phi_{\max}^{\text{ex.2}} = -34.6^\circ$ with the same value of the maximum. Thus, the radiation pattern is symmetric about the plane of symmetry of the antenna. This behavior of the directivity is explained by the fact that the scattering coefficients of azimuthal harmonics with the same absolute value of azimuthal indices m in the isotropic case have equal magnitudes:

$$|D_m| = |D_{-m}|. \tag{15}$$

The mentioned disadvantages of the antenna with isotropic scatterer disappear when a cylindrical scatterer is filled with gyrotropic media. Figure 2(b) shows several directivities obtained for the cases of gyrotropic media of layers of the cylinder. The found elements of the permittivity tensor are given in Table II. As it can be seen from Fig. 2(b), for all given examples, each directivity has only a single main lobe and this lobe has a desired direction. This circumstance is a consequence of the nonreciprocal properties of gyrotropic media, which lead to the failure of the relation (15). Note that the permittivity tensors, which correspond to examples 1 and 7 of Figs. 2(a) and 2(b), are the same. Moreover, the maxima of directivities of Fig. 2(b) are slightly higher than the ones of Fig. 2(a) (except examples 1 and 7).

Obviously, the total field radiated by the magnetic-current filament in the presence of a multilayer gyrotropic cylinder differs significantly from that in the case where the cylindrical scatterer is filled with isotropic media. Figures 3(a) and 3(b) respectively show near- and midfield structures of the absolute value of the total magnetic field that normalized to I_0, $10\log_{10}|H_z|$, in the case of the isotropic filling media which corresponds to example 4 of Fig. 2(a). The field has the form of a standing wave along the angular coordinate with the dominance of azimuthal harmonics $m = \pm 4$. It can be seen in the midfield distribution that the main beams in the directions $\phi = \pm 90^\circ$ are becoming dominant, and the side beams are disappearing. As it is clear from Figs. 3(c) and 3(d), which are plotted at the parameters of the cylinder of example 4 of Fig. 2(b), the total field structure in the case of the gyrotropic cylinder differs significantly from the isotropic one. So that in the near-field zone, the magnitude H_z has mostly the uniform angular distribution, despite the dominance of the azimuthal harmonics of the scattered field $m = 1, \pm 3$, and -5. The midfield distribution in the gyrotropic case shown in Fig. 3(d) has a nonsymmetric structure with a weakly viewed main beam in the direction $\phi = 90^\circ$. The near- and midfield structures of the absolute value of the total magnetic field for other examples given in Tables I and II are shown in Figs. 5, 6, and 7 in Appendix B.

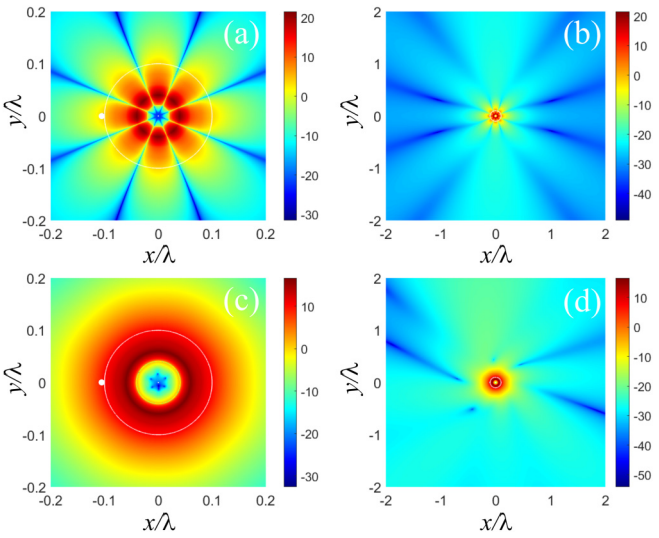

FIG. 3. Value of $10\log_{10}|H_z|$ for the five-layer cylinder: panels (a) and (b) for the case of the isotropic filling media and panels (c) and (d) for the case of the gyrotropic filling media. Both cases correspond to example 4 of Fig. 2. The white circumferences show the outer boundary of the cylinders and the white dots indicate the field source position.

The abovementioned features of the field can also affect the behavior of the Poynting vector and the angular momentum of the total field. Consider the time-averaged angular momentum of the field with respect to the cylinder axis per unit length along the z axis on the surface of radius ρ which is written as (see details in Appendix C)

$$M_z = \int_0^{2\pi} L_z d\phi, \tag{16}$$

where

$$L_z = -\frac{1}{2c^2}\rho^2 \text{Re}(E_{\rho;\Sigma} H_{z;\Sigma}^*), \tag{17}$$

where $E_{\rho;\Sigma}$ and $H_{z;\Sigma}$ are the components of the total field, and the asterisk denotes complex conjugation. Figure 4 shows the dependences of the value L_z on the angle ϕ in the far zone in the cases of the isotropic and gyrotropic cylinders (solid and dashed lines, respectively), which correspond to examples 4 of Fig. 2. It can be seen that in the case of the isotropic cylinder, the dependence of L_z on the angle ϕ is antisymmetric with respect to the plane of symmetry of the antenna, so that the angular momentum M_z is zero. At the same time, the dependence of L_z on the angle ϕ of the gyrotropic antenna has the difficult behavior and the angular momentum $M_z = -4.3/(k_0^2 c^2 Z_0)$. Thus, in the case of an antenna with a gyrotropic scatterer, the radiated waves carry not only the energy from the radiating system but also the angular momentum. This property of the considered antenna may be useful for its orientation in space due to the transfer of this angular momentum (with the opposite sign) to the radiating system.

Note the following remarks on this work. First, in the given article, we considered lossless media, but as it has been shown in the recent work [30], even taking into account losses in

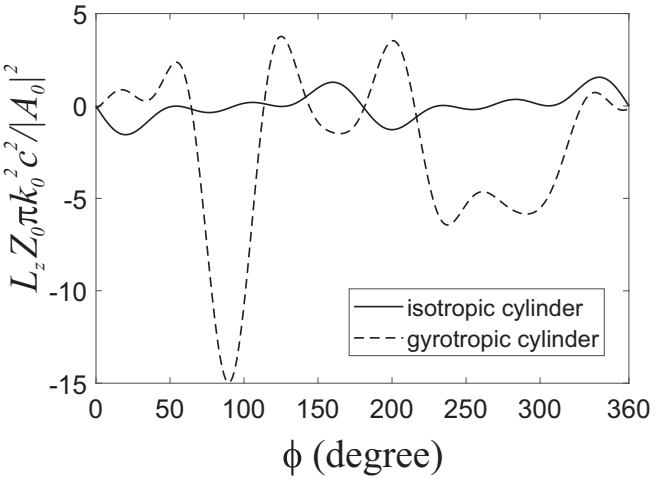

FIG. 4. Dependences of L_z given by Eq. (17) on the angle ϕ in the far-zone in the cases of the isotropic and gyrotropic cylinders of example 4 of Fig. 2. The solid and dashed lines correspond to the isotropic and gyrotropic cylinders, respectively.

the media of cylinder layers, it is possible to choose a set of parameters at which the antenna remains superdirectional. Moreover, in some cases, the presence of losses in media can lead to an increase in the radiation performance of the considered antenna system (see the example in Appendix D). Second, the absolute values of the elements of permittivity tensor (1) were limited by 50 at the optimization procedure. However, these elements can reach much higher values in the resonance frequency ranges of gyrotropic media [21,27], which expands the possibilities for improving the desired antenna performance significantly. Third, the variation in an external static magnetic field can lead to changes in the parameters of gyrotropic media and, consequently, to changes in the radiation pattern of the source considered. This feature can be beneficial in applications requiring a variation in antenna radiation characteristics.

IV. CONCLUSIONS

In this article, the radiation from the filamentary magnetic-current sources in the presence of a multilayer isotropic or a gyrotropic cylindrical scatterer located in the surrounding free space has been studied. It has been demonstrated that a radiating system consisting of a magnetic-current filament and a multilayer gyrotropic cylinder with an electrically small outer radius can have a directivity pattern that cannot be realized in the case of an antenna with a multilayer isotropic cylinder. The results obtained can be useful in many applications functioning in optical and microwave frequency ranges such as subwavelength imaging, wireless communication systems, and photonic integrated circuits.

ACKNOWLEDGMENT

This work was supported by the Russian Science Foundation (Project No. 18-72-10046).

APPENDIX A: RADIATED POWER

The time-averaged Poynting vector in the outer region of the cylinder ($\rho > \rho_N$) can be written as

$$\mathbf{S} = \tfrac{1}{2}\mathrm{Re}[\mathbf{E}_\Sigma \times \mathbf{H}_\Sigma^*], \tag{A1}$$

where $\mathbf{E}_\Sigma = \mathbf{E}^{(f)} + \mathbf{E}^{(s)}$, $\mathbf{H}_\Sigma = \mathbf{H}^{(f)} + \mathbf{H}^{(s)}$, and the asterisk denotes complex conjugation. Consider the time-averaged total radiated power in the radial direction in the far zone ($k_0\rho \gg 1$). This term per unit length along the z axis can be written as

$$P = \int_0^1 dz \int_0^{2\pi} \mathbf{S}\hat{\rho}_0 \rho d\phi. \tag{A2}$$

After substituting Eq. (A1) into Eq. (A2), we have the following expression:

$$P = \frac{1}{2}\int_0^{2\pi} \mathrm{Re}(E_{\phi;\Sigma} H_{z;\Sigma}^*)\rho d\phi. \tag{A3}$$

Here

$$E_{\phi;\Sigma} = i\sum_{m=-\infty}^{\infty} [A_m J_m(k_0\rho_{0s}) + D_m] H_m^{(2)'}(k_0\rho)\exp(-im\phi),$$

$$H_{z;\Sigma} = Z_0^{-1}\sum_{m=-\infty}^{\infty} [A_m J_m(k_0\rho_{0s}) + D_m] H_m^{(2)}(k_0\rho)\exp(-im\phi).$$

Using the approximation of the Hankel function for the large argument [28], we have the following expressions for the field components:

$$E_{\phi;\Sigma} \simeq \sqrt{\frac{2}{\pi k_0\rho}}\exp[-i(k_0\rho - \pi/4)] \times \sum_{m=-\infty}^{\infty} i^m [A_m J_m(k_0\rho_{0s}) + D_m]\exp(-im\phi),$$

$$H_{z;\Sigma} \simeq Z_0^{-1}\sqrt{\frac{2}{\pi k_0\rho}}\exp[-i(k_0\rho - \pi/4)] \times \sum_{m=-\infty}^{\infty} i^m [A_m J_m(k_0\rho_{0s}) + D_m]\exp(-im\phi).$$

After integrating, we have

$$P = \frac{2}{k_0 Z_0}\sum_{m=-\infty}^{\infty} |A_m J_m(k_0\rho_{0s}) + D_m|^2. \tag{A4}$$

The directivity of the considered case is given by the formula (see Refs. [15,31])

$$D(\phi) = \frac{1}{2}\frac{\rho \mathrm{Re}(E_{\phi;\Sigma} H_{z;\Sigma}^*)}{P/(2\pi)}. \tag{A5}$$

After simplification, we have Eq. (14).

APPENDIX B: NUMERICAL CALCULATIONS

1. Optimization procedure

The finding of the optimal parameters of the media of the cylinder layers at which the maximum directivity in the desired $\phi_{\max}$ direction is achieved was based on using the *fmincon* function of the MATLAB software packages.

Five diagonal elements (ε_j) and five off-diagonal elements (g_j) of the layers were optimized to allow the desired directivity. The optimization routine used the fmincon function of MATLAB as follows:

`[x, f]=fmincon(fun,x0,A,b,Aeq,beq,lb,ub).`

Here `x` are the optimized values of the elements of the permittivity tensors ($\mathtt{x} = [\varepsilon_1, g_1, \varepsilon_2, g_2, \ldots, \varepsilon_5, g_5]$); `f` is the minimized value of the cost function; `fun` is the function to minimize, which was determined as

$$\mathtt{fun} = \frac{1}{D(\phi_{\max})} \tag{B1}$$

[here $D(\phi)$ is given by Eq. (14) and $\phi_{\max}$ is desired direction of directivity]; $\mathtt{x0} = [\varepsilon_{10}, g_{10}, \varepsilon_{20}, g_{20}, \ldots, \varepsilon_{50}, g_{50}]$ are the initial values; `lb` and `ub` are the lower and upper bounds of optimized values, respectively, ($\mathtt{lb} = [-50, -50, \ldots, -50]$, $\mathtt{ub} = [50, 50, \ldots, 50]$); and other parameters (`A,b,Aeq,beq`) are replaced with empty values. Note, the optimization procedure was carried out without taking into account the off-diagonal elements, which were taken as zeros, for isotropic media of the cylinder.

Because the function (B1) has many local minima, different initial points can lead to different solutions. Therefore, optimal values were found with brute-forcing on the initial values. The initial points were calculated as

$$\begin{aligned}
&\mathtt{x0} = \mathtt{n}*[\varepsilon_{10}, g_{10}, \varepsilon_{20}, g_{20}, \varepsilon_{30}, g_{30}, \varepsilon_{40}, g_{40}, \varepsilon_{50}, g_{50}],\\
&\varepsilon_{10} = (-1)^{\mathtt{mod(p,2)}}, \quad \varepsilon_{20} = (-1)^{\mathtt{fix(p,2)}},\\
&\varepsilon_{30} = (-1)^{\mathtt{fix(p,4)}}, \quad \varepsilon_{40} = (-1)^{\mathtt{fix(p,8)}},\\
&\varepsilon_{50} = (-1)^{\mathtt{fix(p,16)}}, \quad g_{10} = \varepsilon_{10}/2, \quad g_{20} = \varepsilon_{20}/2,\\
&g_{30} = \varepsilon_{30}/2, \quad g_{40} = \varepsilon_{40}/2, \quad g_{50} = \varepsilon_{50}/2.
\end{aligned}$$

Here $\mathtt{n} = -30, -29, \ldots, -1, 1, \ldots, 29, 30$; `mod` is the function returning remainder after division; `fix` is the function returning round toward zero after division; and $\mathtt{p} = 0, 1, 2, \ldots, 2^5 - 1$. During optimization, two loops are performed by parameters `n` and `p` for changing the initial points. At the end, among all the found sets of values, the combination of parameters is selected for which the directivity is maximal.

The numerical calculations were carried out for a five-layer cylindrical scatterer, whose exterior radius has a value of $\rho_5 = 0.1\lambda$ and the inner radii were fixed on values $\rho_1 = 0.02\lambda$, $\rho_2 = 0.04\lambda$, $\rho_3 = 0.06\lambda$, and $\rho_4 = 0.08\lambda$. The magnetic-current filament was located at the distance $\rho_{0s} = 1.05\rho_5$ from the axis of a cylindrical scatterer and at an angle $\phi_{0s} = 180^\circ$. The magnitudes of azimuthal indexes were limited with a value of 5 ($m = 0, \pm 1, \ldots, \pm 5$).

2. Isotropic cylinder

The permittivities of media of layers of an isotropic cylinder for which the directivity of the antenna has maxima value are given in Table I. Figures 5(a) and 5(b) respectively show near- and midfield structures of the absolute value of the total magnetic field, $10\log_{10}|H_z|$, in the case of the isotropic filling media which corresponds to example 1 of Table I. Figures 5(c) and 5(d) show the same quantities as in Figs. 5(a) and 5(b), but for example 7 of Table I. The left and right columns of Fig. 6 show the same quantities as the left and right columns of Fig. 5, respectively, but for the 2nd example [Figs. 6(a) and 6(b)], the 3rd example [Figs. 6(c) and 6(d)], the 5th example [Figs. 6(e) and 6(f)], and the 6th example [Figs. 6(g) and 6(h)] of Table I.

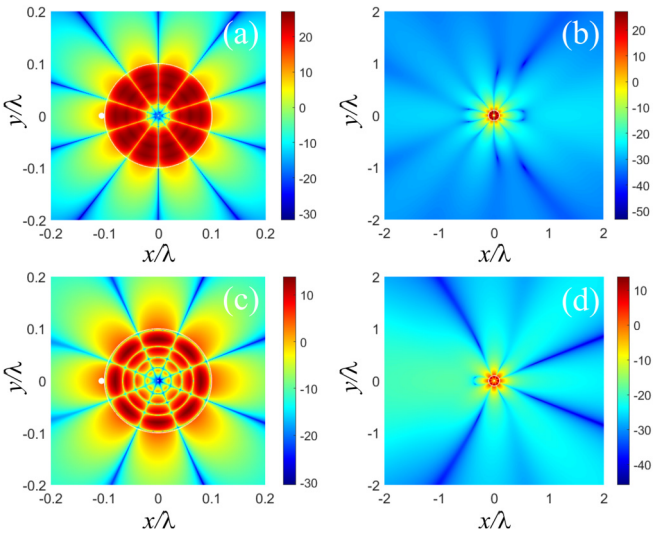

FIG. 5. Value of $10\log_{10}|H_z|$ for the five-layer cylinder in the case of the isotropic filling media. Panels (a) and (b) correspond to the 1st example, and panels (c) and (d) correspond to the 7th example in Table I (and the same examples of Table II). The white circumferences show the outer boundary of the cylinders and the white dots indicate the source position.

3. Gyrotropic cylinder

The elements of permittivity tensors of media of layers of a gyrotropic cylinder with the maximum values of directivity of the antenna are given in Table II. The left and right columns of Fig. 7 show field distributions as the left and right columns of Fig. 5, respectively, but for the 2nd example [Figs. 7(a) and 7(b)], the 3rd example [Figs. 7(c) and 7(d)], the 5th example [Figs. 7(e) and 7(f)], and the 6th example [Figs. 7(g) and 7(h)] of Table II.

APPENDIX C: ANGULAR MOMENTUM

The time-averaged angular-momentum density is (see in Ref. [32])

$$\mathbf{m} = \frac{1}{2c^2}\mathrm{Re}[\mathbf{r} \times (\mathbf{E}_\Sigma \times \mathbf{H}_\Sigma^*)]. \tag{C1}$$

TABLE I. The elements of the permittivity tensors (1) of the case of the isotropic media of layers of the cylinder. The first column contains the number of examples marked in Fig. 2(a), and the second column contains desired directions of the maximum radiation.

No.	$\phi_{\max}$	ε_1	ε_2	ε_3	ε_4	ε_5
1	0°	12.223	−49.921	21.902	−19.998	35.840
2	30°	2.658	−30.427	8.080	−7.568	31.564
3	60°	−14.320	19.475	−21.209	4.038	30.817
4	90°	−0.072	−1.501	1.538	0.499	1.364
5	120°	−40.651	8.587	−6.680	40.762	−0.576
6	150°	−20.599	17.068	−27.717	20.896	25.812
7	180°	−1.422	2.004	−4.325	9.562	−9.861

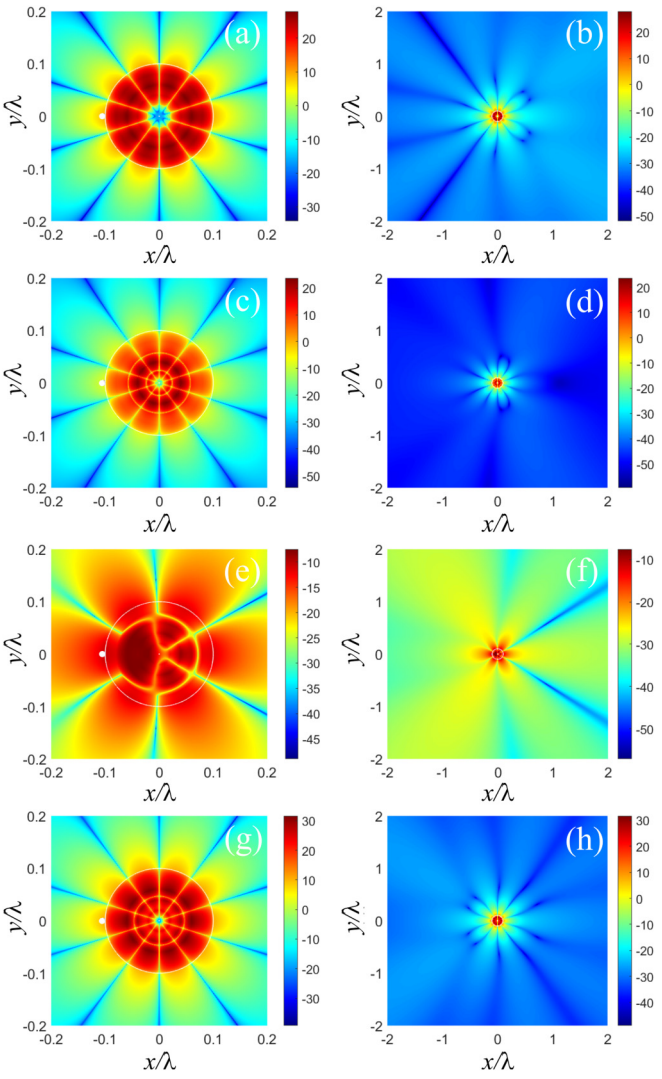

FIG. 6. Value of $10\log_{10}|H_z|$ for the five-layer cylinder in the case of the isotropic filling media. Panels (a) and (b) correspond to the 2nd example, panels (c) and (d) correspond to the 3rd example, panels (e) and (f) correspond to the 5th example, and panels (g) and (h) correspond to the 6th example in Table I. The white circumferences show the outer boundary of the cylinders and the white dots indicate the source position.

The total time-averaged angular-momentum is

$$\mathbf{J} = \int \mathbf{m} d\mathbf{r}. \tag{C2}$$

The time-averaged angular momentum of field with respect to the cylinder axis per unit length along the z axis on a surface of radius ρ is written as

$$M_z = \int_0^1 dz \int_0^{2\pi} m_z \rho d\phi. \tag{C3}$$

In the considered system only the longitudinal component is nonzero. It is rewritten as

$$M_z = \int_0^{2\pi} L_z(\phi) d\phi, \tag{C4}$$

where

$$L_z(\phi) = -\frac{1}{2c^2}\mathrm{Re}(E_{\rho;\Sigma} H^*_{z;\Sigma})\rho^2. \tag{C5}$$

In the far zone, Eq. (C5) is rewritten as

$$L_z(\phi) = \frac{1}{Z_0 \pi k_0^2 c^2} \times \mathrm{Re}\left[\left(\sum_{m=-\infty}^{\infty} m i^m [A_m J_m(k_0\rho_{0s}) + D_m]\exp(-im\phi)\right) \times \left(\sum_{m=-\infty}^{\infty} i^m [A_m J_m(k_0\rho_{0s}) + D_m]\exp(-im\phi)\right)^*\right] \tag{C6}$$

After integration of Eq. (C4) in the far zone, we have

$$M_z = \frac{2}{Z_0 k_0^2 c^2} \sum_{m=-\infty}^{\infty} m |A_m J_m(k_0\rho_{0s}) + D_m|^2. \tag{C7}$$

APPENDIX D: ABOUT THE POSSIBILITY OF INCREASING OF DIRECTIVITY IN THE PRESENCE OF LOSSES IN MEDIA

Consider the case of the scatterer in which gyrotropic media of the cylinder layers are lossy media. The elements of the permittivity tensor (1) of the medium of the jth layer have real and imaginary parts:

$$\varepsilon_j = \varepsilon'_j - i\varepsilon''_j \quad g_j = g'_j + ig''_j, \quad \eta_j = \eta'_j - i\eta''_j. \tag{D1}$$

Here the values ε''_j, g''_j, and η''_j are not less than zero. For simplicity we assume that the imaginary parts of the tensor

TABLE II. The elements of the permittivity tensors (1) of the case of the gyrotropic media of layers of the cylinder. The first column contains the number of examples marked in Fig. 2(b), and the second column contains desired directions of the maximum radiation.

No.	$\phi_{\max}$	ε_1	g_1	ε_2	g_2	ε_3	g_3	ε_4	g_4	ε_5	g_5
1	0°	12.223	0	−49.921	0	21.902	0	−19.998	0	35.840	0
2	30°	−21.319	8.603	0.195	1.214	−49.587	3.213	31.007	−5.045	21.329	7.652
3	60°	27.947	12.954	−24.091	−18.749	−30.633	−12.680	−12.651	8.042	36.491	11.617
4	90°	−11.796	1.809	−2.014	0.598	15.420	5.772	7.301	−6.791	−0.444	0.159
5	120°	−20.605	6.345	−29.547	12.126	−2.564	−0.527	12.812	5.130	−15.080	−12.716
6	150°	−6.928	−10.320	−9.377	−1.668	−2.972	0.127	13.518	9.118	−5.895	−2.166
7	180°	−1.422	0	2.004	0	−4.325	0	9.562	0	−9.861	0

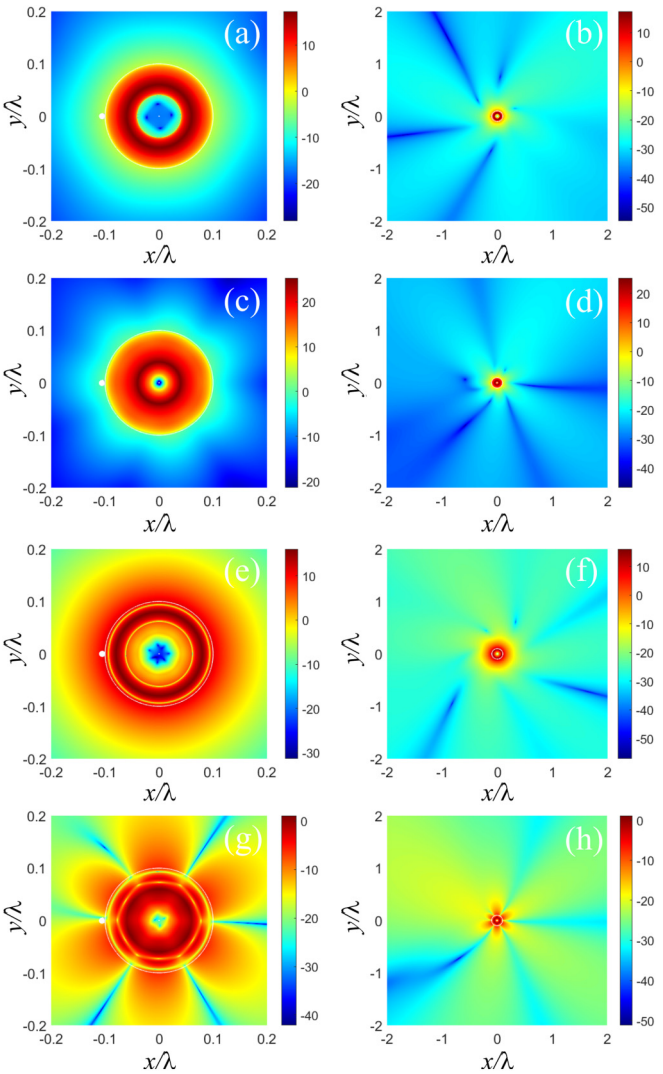

FIG. 7. Value of $10\log_{10}|H_z|$ for the five-layer cylinder in the case of the gyrotropic filling media. Panels (a) and (b) correspond to the 2nd example, panels (c) and (d) correspond to the 3rd example, panels (e) and (f) correspond to the 5th example, and panels (g) and (h) correspond to the 6th example in Table II. The white circumferences show the outer boundary of the cylinders and the white dots indicate the source position.

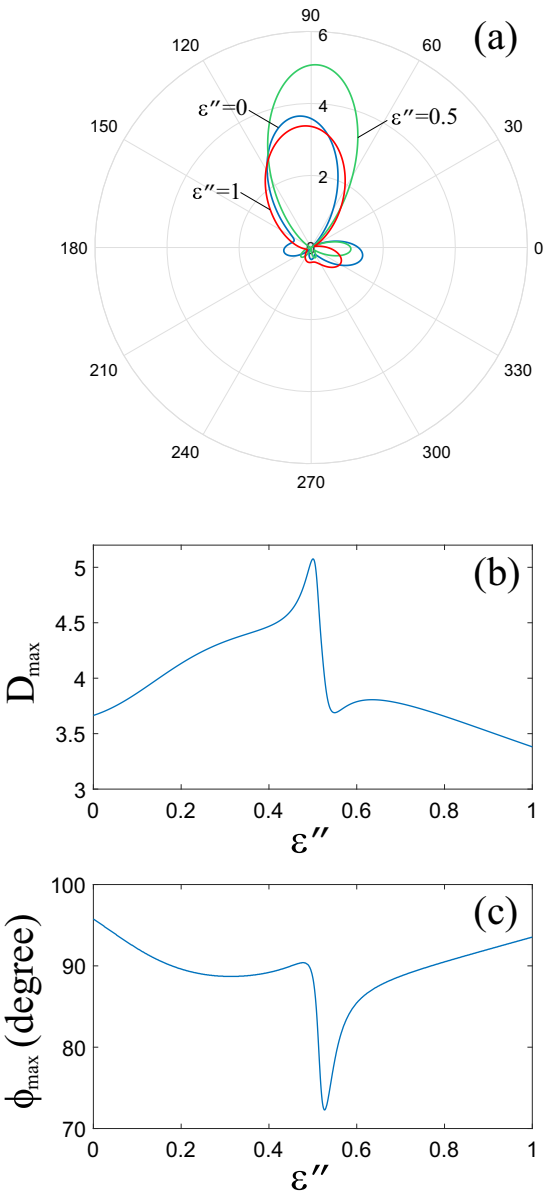

FIG. 8. (a) Directivities were obtained for the case of the lossy and lossless gyrotropic media of layers of the cylinder. Dependences of maximum of directivity (b) and direction of the main lobe (c) on ε''.

elements among all layers are identical and equal to ε'', so that $\varepsilon_j'' = \varepsilon''$, $g_j'' = \varepsilon''$, and $\eta_j'' = \varepsilon''$.

As in the main part of this work, we consider the five-layer cylinder. Numerical calculations have been carried out at fixed real parts of the elements of the permittivity tensor of the media which had the following values:

$$\varepsilon_1 = -22.975,\ g_1 = 5.064,\ \varepsilon_2 = -19.78,\ g_2 = -10.562,$$
$$\varepsilon_3 = -30.171,\ g_3 = 9.913,\ \varepsilon_4 = 10.187,\ g_4 = -7.43,$$
$$\varepsilon_5 = 45.569,\ g_5 = -23.219.$$

Figure 8(a) shows several directivities obtained for the cases of absence and presence ($\varepsilon_j'' = 0.5$ and $\varepsilon_j'' = 1$) of losses in the gyrotropic media of layers of the cylinder. The greatest directivity among these three cases is achieved with losses in the medium equal to 0.5. Wherein the main lobe is directed at an angle of $\phi = 90^\circ$. Moreover, it follows from Fig. 8 [which shows the dependences of the maximum of directivity $D_{\max}$ (b) and direction of the main lobe (c) on ε''] that $\varepsilon'' = 0.5$ corresponds to the case of the best directivity. The nonlinear dependence of $D_{\max}$ on ε'' is explained by changes of the contributions of the azimuthal harmonics of the scattered field in the total field. Note that the nonmonotonic dependence of the scatterer parameters on losses in the medium was previously observed for efficient absorption of electromagnetic energy by nanoparticles, including core-shell nanoparticles [33].

[1] R. W. Ziolkowski and N. Engheta, IEEE Trans. Anten. Propag. **68**, 1232 (2020).
[2] L. Novotny and N. Van Hulst, Nat. Photon. **5**, 83 (2011).
[3] A. E. Krasnok, I. S. Maksymov, A. I. Denisyuk, P. A. Belov, A. E. Miroshnichenko, C. R. Simovski, and Y. S. Kivshar, Phys.-Usp. **56**, 539 (2013).
[4] F. Monticone and A. Alu, Rep. Prog. Phys. **80**, 036401 (2017).
[5] A. F. Koenderink, ACS Photon. **4**, 710 (2017).
[6] A. F. Cihan, A. G. Curto, S. Raza, P. G. Kik, and M. L. Brongersma, Nat. Photon. **12**, 284 (2018).
[7] A. Alù and N. Engheta, Phys. Rev. Lett. **104**, 213902 (2010).
[8] D. Dregely, K. Lindfors, M. Lippitz, N. Engheta, M. Totzeck, and H. Giessen, Nat. Commun. **5**, 4354 (2014).
[9] S. Kawata, Y. Inouye, and P. Verma, Nat. Photon. **3**, 388 (2009).
[10] E. Khoram, A. Chen, D. Liu, L. Ying, Q. Wang, M. Yuan, and Z. Yu, Photon. Res. **7**, 823 (2019).
[11] R. W. Ziolkowski, Phys. Rev. X **7**, 031017 (2017).
[12] A. Alu and N. Engheta, IEEE Trans. Anten. Propag. **55**, 3027 (2007).
[13] W. Liu, J. Zhang, B. Lei, H. Ma, W. Xie, and H. Hu, Opt. Express **22**, 16178 (2014).
[14] A. E. Krasnok, C. R. Simovski, P. A. Belov, and Y. S. Kivshar, Nanoscale **6**, 7354 (2014).
[15] S. Arslanagić and R. W. Ziolkowski, Phys. Rev. Lett. **120**, 237401 (2018).
[16] W. Chen, J. Fu, Q. Wu, and B. Lv, J. Phys. D: Appl. Phys. **52**, 495102 (2019).
[17] W. Chen, J. Fu, B. Lv, and Q. Wu, Appl. Opt. **59**, 8302 (2020).
[18] T. Zhang, X. Li, J. Xu, X. Zhang, Z. L. Deng, and X. Li, Nanomaterials **10**, 1242 (2020).
[19] V. A. Es'kin, A. V. Ivoninsky, A. V. Kudrin, and L. L. Popova, J. Exp. Theor. Phys. **124**, 202 (2017).
[20] V. A. Es'kin, A. V. Ivoninsky, A. V. Kudrin, and C. Krafft, Phys. Scr. **91**, 15502 (2015).
[21] E. D. Palik, R. Kaplan, R. W. Gammon, H. Kaplan, R. F. Wallis, and J. J. Quinn, Phys. Rev. B **13**, 2497 (1976).
[22] E. Moncada-Villa, V. Fernández-Hurtado, F. J. García-Vidal, A. García-Martín, and J. C. Cuevas, Phys. Rev. B **92**, 125418 (2015).
[23] S. Pakniyat, Y. Liang, Y. Xiang, C. Cen, J. Chen, and G. W. Hanson, J. Appl. Phys. **128**, 183101 (2020).
[24] F. Capolino, *Theory and Phenomena of Metamaterials* (CRC Press, Boca Raton, FL, 2017).
[25] I. Tralle, P. Zięba, and W. Paśko, J. Appl. Phys. **115**, 233509 (2014).
[26] V. L. Ginzburg, *The Propagation of Electromagnetic Waves in Plasmas* (Pergamon Press, Oxford, 1970).
[27] I. G. Kondrat'ev, A. V. Kudrin, and T. M. Zaboronkova, *Electrodynamics of Density Ducts in Magnetized Plasmas* (Gordon and Breach, Amsterdam, 1999).
[28] M. Abramowitz and I. A. Stegun, *Handbook of Mathematical Functions with Formulas, Graphs, and Mathematical Tables* (National Bureau of Standards, Washington, DC, 1972).
[29] M. Shafa, S. Akbar, L. Gao, M. Fakhar-e-Alam, and Z. M. Wang, Nanoscale Res. Lett. **11**, 164 (2016).
[30] W. Chen, J. Fu, B. Lv, and Q. Wu, J. Phys. D: Appl. Phys. **53**, 405105 (2020).
[31] C. A. Balanis, *Antena Theory: Analysis and Design* (Wiley, New York, 2016).
[32] J. D. Jackson, *Classical Electrodynamics* (Wiley, New York, 1998).
[33] B. S. Luk'yanchuk, A. E. Miroshnichenko, M. I. Tribelsky, Y. S. Kivshar, and A. R. Khokhlov, New J. Phys. **14**, 093022 (2012).